Available online at www.sciencedirect.com

ScienceDirect

Publishing Services by Elsevier

International Journal of Naval Architecture and Ocean Engineering 9 (2017) 624–640

http://www.journals.elsevier.com/international-journal-of-naval-architecture-and-ocean-engineering/

Estimation of slamming coefficients on local members of offshore wind turbine foundation (jacket type) under plunging breaker

Jithin Jose [a,*], Sung-Jin Choi [b]

[a] Department of Mechanical and Structural Engineering and Materials Science, University of Stavanger, Norway

[b] Loads Copenhagen, DNV GL, Copenhagen, Denmark

Received 16 September 2016; revised 7 February 2017; accepted 9 March 2017

Available online 6 April 2017

Abstract

In this paper, the slamming coefficients on local members of a jacket structure under plunging breaker are studied based on numerical simulations. A 3D numerical model is used to investigate breaking wave forces on the local members of the jacket structure. A wide range of breaking wave conditions is considered in order to get generalized slamming coefficients on the jacket structure. In order to make quantitative comparison between CFD model and experimental data, Empirical Mode Decomposition (EMD) is employed for obtaining net breaking wave forces from the measured response, and the filtered results are compared with the computed results in order to confirm the accuracy of the numerical model. Based on the validated results, the slamming coefficients on the local members (front and back vertical members, front and back inclined members, and side inclined members) are estimated. The distribution of the slamming coefficients on local members is also discussed.

Keywords: Navier Stokes; Numerical simulation; Wave breaking; Slamming coefficient; Jacket

1. Introduction

Due to the increased energy demand and thrive for clean energy, offshore wind energy has become popular these days. A large number of offshore wind turbines are been supported by fixed type substructures (e.g., monopile, gravity foundations, tripod, or jacket type). Among these, the monopile structures are generally used because of simplicity in the design and installation. However, the increase in the turbine capacity and feasibility of fixed type Offshore Wind Turbine (OWT) in deeper water depths made the industry to focus more on rigid type of substructures, such as jacket type structures.

Most of the existing offshore wind turbine substructures are installed in relatively shallow water in order to reduce the cost of fabrication, maintenance and grid connectivity. However, in case where the substructures are installed in shallow waters where wave breaking occurs (e.g., Thornton bank wind farm near Belgian coast), the breaking waves would give rise to serious damages to the substructure. Since the wave-breaking phenomenon is extremely complicated and involve strong non-linear effect, the breaking wave forces would be one of the major concerns in the design of these OWT substructures.

Till date, a semi-empirical formula has been used to calculate the breaking wave forces on monopile structures (Goda et al., 1966). The slamming coefficient used in the semi-empirical formula should be determined in advance, based on the previous researches. Many researches have been done in past to estimate the slamming coefficients (Goda et al., 1966; Sawaragi and Nochino, 1984; Wienke and Oumeraci, 2005) valid for monopile structures. However, it is revealed that there is a major uncertainty in the value of slamming

* Corresponding author.
E-mail address: jithin.jose@uis.no (J. Jose).

Peer review under responsibility of Society of Naval Architects of Korea.

http://dx.doi.org/10.1016/j.ijnaoe.2017.03.006

coefficients, which is to be used for the calculation of breaking wave forces on monopile structures using the semi-empirical formula. For example, the slamming coefficients estimated by different researchers showed a considerable degree of scatter (from 3.14 to 6.28). The design guidelines (IEC 61400-3 (2009), ISO 21650 (2007), GL (2005), ABS (2010), DNV-RP-C205 (2010), API RP 2A-WSD (2007) and ISO 19902 (2007)), also shows no exact agreement on the slamming coefficient to be used for the design of such structures. The strong nonlinear wave–structure interactions during the wave breaking and difficulties in the accurate measurement of the breaking waves would make the exact physical representation of breaking waves a challenging task.

In the case of jacket type structures, there have been not many attempts in the past to estimate the breaking wave forces on the structures. In comparison with monopile, the jacket type structures are complex due to more members, joints and different member orientations. Hence, it is important to investigate the slamming coefficients on each local members (e.g., front and back vertical members, front and back inclined piles and lateral inclined member) of the jacket structure in the wave breaking zone. Moreover, the distribution of the slamming coefficients on the local members is important in the design of OWT substructure (e.g., base shear and bending moments). Nevertheless, in the design guidelines (and previous researches), there is limited information on the design of jacket structures against breaking waves.

The WaveSlam project (Arntsen and Gudmestad, 2014; Arntsen et al., 2013) was carried out in 2013, with the aim to investigate the wave forces from plunging breaking waves on a jacket structure in shallow waters. In the experiment, the jacket structure was tested for number of wave breaking cases and the response of the structure was measured. Jose et al. (2016b) performed initial studies on the experimental measurement data and proposed methods to obtain actual breaking wave forces on jacket members from the measured responses. However, the experimental studies have some limitation in terms of the instrumentation to measure the variation of local wave forces along the jacket members.

The development of a Navier Stokes solver to study the breaking wave forces have been an active field of research in recent past (Mo et al., 2013; Lee, 2006; Lee et al., 2011; Christensen et al., 2005; Alagan Chella et al., 2016; Choi et al., 2015). Mo et al. (2007) developed a Navier–Stokes solver to compute the wave–structure interaction on vertical slender pile. Christensen et al. (2005) studied the nonlinear run-up and the breaking wave forces on a cylindrical pile under spilling and plunging breakers using Navier Stokes solver. Kamath et al., 2016 studied breaking wave interactions on a vertical cylinder with respect to different wave breaking positions. They used open source CFD model REEF3D to simulate the breaking wave forces on the vertical cylinder. Choi (2014) and Choi et al. (2015) used a 3D numerical model based on finite difference method to calculate the breaking wave forces on monopile structures. The breaking wave forces on monopile structure at various orientations were simulated in those studies. The numerical results showed good agreement with the experimental measurements. However, most of these studies were limited to monopile structures. As there were limited experimental results available for jacket structures, there have been not many attempts to develop a numerical model to predict the breaking wave forces on the jacket structures.

Recently, Jose et al. (2016a) validated a 3D numerical model with the WaveSlam experimental data for the jacket structures. Based on the numerical simulations, slamming coefficients were estimated for the front and back vertical members of the jacket structure. The maximum slamming coefficient for the vertical members was found to be slightly smaller than the value suggested by Goda et al. (1966). A triangular distribution of wave slamming coefficients on the vertical members was obtained in contrast to the rectangular distribution proposed by Goda et al. (1966) and Wienke and Oumeraci (2005). However, in the research, the simulations were performed for a limited number of wave cases and final values of slamming coefficient could not be ascertained.

The objective of the present study is to estimate the slamming coefficients for the local members of a jacket structure. The present paper is an extension to Jose et al., 2016a. A wide range of breaking wave conditions (from short wave (4.6 s) to long wave (5.55 s)) are considered in order to get generalized slamming coefficients on local members of the jacket structure. In order to make quantitative comparison between experimental and CFD results, empirical mode decomposition (Huang et al., 1999; Choi et al., 2015) is used to filter out the dynamic amplification component in the measured response force time series data and the filtered results are compared with the computed results in order to confirm the accuracy of the numerical model. Based on the validated numerical results, the slamming coefficients on the local members (front and back vertical members, front and back inclined members, and side inclined members) are estimated. The distribution of slamming coefficients on the local members is studied. Moreover, the slamming coefficients obtained from the present study are compared with the values presented in previous studies by other researchers.

2. Model description

2.1. Experimental setup

The WaveSlam experiment was carried out in 2013 at the Large Wave Channel, Hannover, with the aim to study the breaking wave forces on a jacket structure. The truss structure of 1:8 scale was tested for large number of wave breaking conditions (Jose et al., 2016b). The experimental setup is shown in Fig. 1.

The large wave flume in Hannover is of 300 m long, 5 m wide and 7 m depth. The slope of the bottom of the tank is 1:10. The diameters of all the jacket members are 0.14 m. The jacket structure was located at a distance of approximately 200 m from the wave generator. The truss structure was equipped with total and local force transducers to measure the wave forces on the structure. There were wave gauges

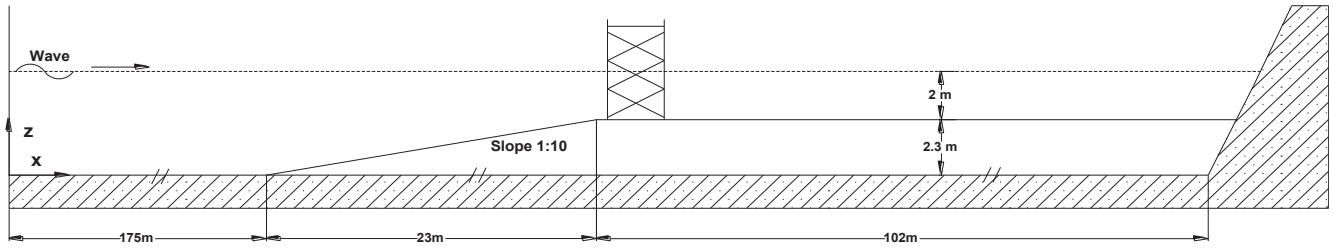

Fig. 1. Experimental set-up on the large wave flume FZK (Arntsen et al., 2013).

distributed along the wave channel to track the wave transformation during the wave breaking. The water particle velocities during the breaking wave were measured using Acoustic Doppler Velocity meter (ADVs) installed in line with the front leg of the truss structure. Fig. 2 shows the instrumented jacket structure in the wave tank.

2.2. Numerical model

2.2.1. Governing equations

When a fluid is modelled as a viscous and incompressible fluid with constant density, the fluid motion can be described by the continuity equation (Eq. (1)) and the modified Navier–Stokes equation (Eq. (2)). The free surface is governed by the Volume of Fluid (VOF) function (F) in Eq. (3) (Choi, 2014).

$$\frac{\partial(mv_j)}{\partial x_j} = q^* \tag{1}$$

$$m\frac{\partial v_i}{\partial t} + mv_j\frac{\partial v_i}{\partial x_j} = \frac{-m}{\tilde{\rho}}\frac{\partial p}{\partial x_i} + \frac{\partial}{\partial x_j}\left(2\tilde{\nu}D_{ij} - \tau_{ij}\right) - Q_i - \beta_{ij}v_j + f_i \tag{2}$$

$$\frac{\partial(mF)}{\partial t} + \frac{\partial(mv_jF)}{\partial x_j} = Fq^* \tag{3}$$

where, t is the time; $v_i = [u, v, w]^T$ is the velocity vector; p is pressure; $x_i = [x, y, z]^T$ is the position vector; is the ratio of the fractional area open to the flow; m is the arbitrary body forces due to the effects of gravity and surface tension; $D_{ij} = (\partial v_i/\partial x_j + \partial v_j/\partial x_i)/2$ is the strain rate tensor; τ_{ij} is the turbulent stress based on the Smagorinsky SGS (sub-grid scale) model; $\beta_{ij} = \beta\delta_{i3}\delta_{j3}$ is the dissipation factor matrix, in which β is the dissipation factor that equals 0, except in the added dissipation zone; $q^* = q(y, z; t)/\Delta x_s$ is the wave generation source, where $q(y, z; t)$ is the source density assigned only at the source position $(x = x_s)$ and Δx_s is the mesh width at the source position; $\tilde{\rho}$ and $\tilde{\nu}$ are the density and the kinematic viscosity averaged over the computational grid, respectively; F is the VOF function and Q_i is the wave source vector.

An application based on cut cell method is used to install the complex geometries (e.g., Jacket structure and bottom slope) in the computational domain. For the discretization of the continuity equation, the central difference scheme is used. In the discretization of Navier Stokes equations, the forward difference scheme for time derivative terms, the hybrid scheme (the combination of central difference scheme and upwind difference scheme) for advection terms and the central difference scheme for non-advection terms are employed. The Simplified Maker and Cell (SMAC) method (Amsden and Harlow, 1970) is incorporated for the velocity and pressure correction. In order to solve the Poisson pressure equation, an algebraic multi grid (AP-AMG) solver developed by Allied Engineering Corporation (2011) is used.

In the numerical model, the small-scale turbulence generated during the wave breaking in the surf zone is modelled using a Smagorinsky SGS (Sub-Grid Scale) model, while the large-scale turbulence is simulated by solving the governing equations.

Fig. 2. Instrumented jacket structure in the wave tank. Total force transducers are marked by red circles.

As for the boundary conditions, the dynamic boundary condition is automatically satisfied due to the use of a two-phase flow model (i.e., the water and the air phase are modelled as a fluid), while, the kinematic boundary condition is satisfied by tracking the VOF function (Hirt and Nichols, 1981). An impermeable (normal velocities) and a non-slip condition (tangential velocities) are imposed to treat bottom boundary condition and obstacle boundary condition. More details on the numerical model are given in Choi et al. (2015).

2.3. EMD method

The EMD method was developed by Huang et al. (1999), to decompose the given signal in the time domain. It decomposes the signal into number of intrinsic mode functions and a residue. Choi et al. (2015) used the EMD method to filter out the dynamic amplification in the measured response force time series data. Jose et al. (2015) verified the applicability of the EMD method for the total measured forces on the jacket structures. In the present study, the EMD will decompose the measured total response force into an IMF, which will represent the amplified force component due to the structure's vibration and a residue, which is the net breaking wave force.

The various steps in EMD algorithm are:

1) Obtain the upper and lower envelop for the measured force by connecting local maxima and minima, respectively.
2) The extracted local extremes are connected to obtain the upper and lower envelope.
3) The mean of the upper envelope and the lower envelope is obtained, which is the residue and is subtracted from the measured signal to obtain the IMF.
4) The residue represents the net breaking wave force and the IMF represents the amplified component of the force due to the structure's vibration.

2.4. Calculation of slamming coefficients

Fig. 3 shows the locations of the local force transducers on the jacket structure in the CFD model. The local force transducers are distributed along the local members in the global coordinate system. In the numerical model, each local force transducer is described by defining a local region is space around the member. The numerical model identified the wet surface areas in the defined local region and integrated the pressure on these wet surfaces to calculate the local forces. There are 14 local force transducers on each of the bracing members (B1–B6) and 38 force transducers on the front and back vertical members (V1 and V2). The local force transducers on the vertical members are of the size of grid cells (z direction) covering the circumference of the member. The force transducers on the inclined members are formed similar to the vertical force transducers, except that there is a clearance of grid cell between the adjacent transducers. The local wave forces on the jacket members are obtained by direct integration of the pressure distribution along the circumference of the members.

Goda et al. (1966) and Wienke and Oumeraci (2005) proposed a semi-empirical formula (Eq. (4)) to calculate the breaking wave forces on the cylindrical pile.

$$F_s = \frac{1}{2}\rho_w C_s D C_b^2 \lambda \eta_b \tag{4}$$

where, F_s is the total breaking wave force,C_s is the slamming coefficient; C_b is the breaking wave celerity, λ is the curling factor; η_b is the breaking wave height; ρ_w is the water density; D is the diameter of the cylinder.

Eq. (4) is proved to be a good approximation for calculating the breaking wave forces on the cylindrical pile except the uncertainty in the slamming coefficient to the used. Moreover,

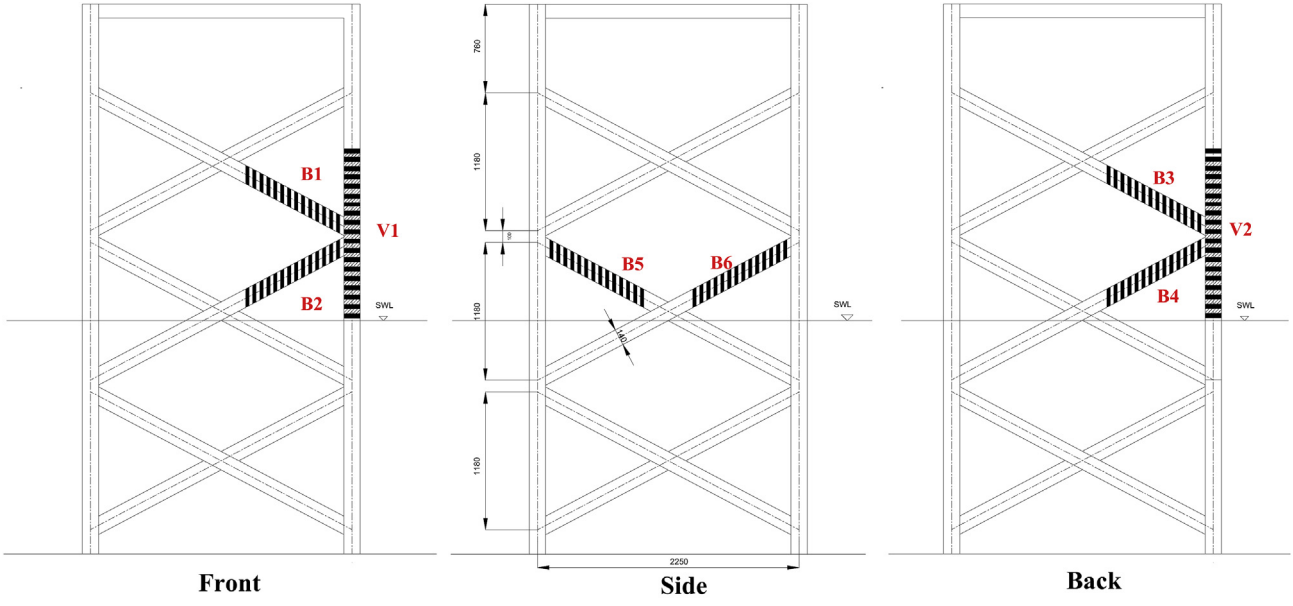

Fig. 3. Locations of the local force transducers on the Jacket structure in the CFD model.

Table 1
Incident wave conditions.

Case	Type	Wave height (m)	Wave period (s)	Water depth (m)
a1	Non-breaking	0.75	4.00	4.3
b1	Breaking	1.50	5.55	4.3
b2		1.60		
b3		1.70		
c1	Breaking	1.50	5.20	4.3
c2		1.60		
c3		1.70		
d1	Breaking	1.50	4.90	4.3
d2		1.60		
d3		1.70		
e1	Breaking	1.50	4.60	4.3
e2		1.60		
e3		1.70		

according to Tanimoto et al. (1986) and Wienke and Oumeraci (2005), Eq. (4) can also be used for inclined piles by changing some parameters. As the maximum slamming force is expected at the time of the impact (t = 0), the slamming coefficients are estimated for the maximum forces calculated by the local force transducers. The projected area is same as the projected area of the local force transducers. The breaking wave celerity is taken directly from the numerical model.

By using Eq. (4), the slamming coefficients for the local force transducers are estimated as,

$$C_s = \frac{2f_l}{\rho_w C_b^2 A_P} \tag{5}$$

A_P is the projected area of the local force transducer; f_l is the maximum slamming force computed by the local force transducers. The projected area A_P, is different for vertical and inclined members of the jacket structure.

2.5. Application of 3D numerical model

A numerical wave tank (NWT) similar to WaveSlam experimental setup is developed. The NWT has a length of 50.0 m, a width of 5.0 m, and a height of 7.0 m. The jacket structure and bottom geometry are modelled in the NWT by considering the x−z plane of symmetry. Only half of the structures is modelled in order to reduce the computational time. The total forces on the structure are calculated by multiplying the forces acting on the half of the structure with a factor 2. The water depths at the wave generator and at the plateau are 4.3 m and 2.0 m, respectively. The jacket structure is located near the edge of the slope. The slope of the bottom is considered to be 1/10.

In order to suppress the internal waves and reflected waves in the NWT, numerical dissipation zones are provided on the left and right side of the computational domain. The length of the dissipation zone is twice the wavelength. The internal wave generator is located on the left side of the computational domain to generate the regular wave train, using a stream function wave theory. Total 13 incident wave conditions are used for making breaking waves in front of, in the middle of, and in the rear of the structure (see Table 1). The free surface elevation and water particle velocities are calculated by the numerical gauges (wave gauges (WG1−WG6) and velocity gauges (VG1 and VG2)) distributed in NWT similar to the experimental setup (see Fig. 4). In the CFD model, the total breaking wave forces on the jacket structure are obtained by integrating the pressures on the structure. The local breaking wave forces are obtained from the force transducers distributed on the circumference of the members (see Fig. 3) along the length of the member (front, side and back vertical and inclined members). The time increment is automatically adjusted at each time step in order to obtain maximum efficiency. The model is run for 10 wave periods.

3. Results and discussion

In the WaveSlam experiment (Jose et al., 2016b), the jacket structure was tested for number of non-breaking and breaking wave cases. Among them, most of the critical wave cases are simulated in the NWT to get slamming coefficients on local

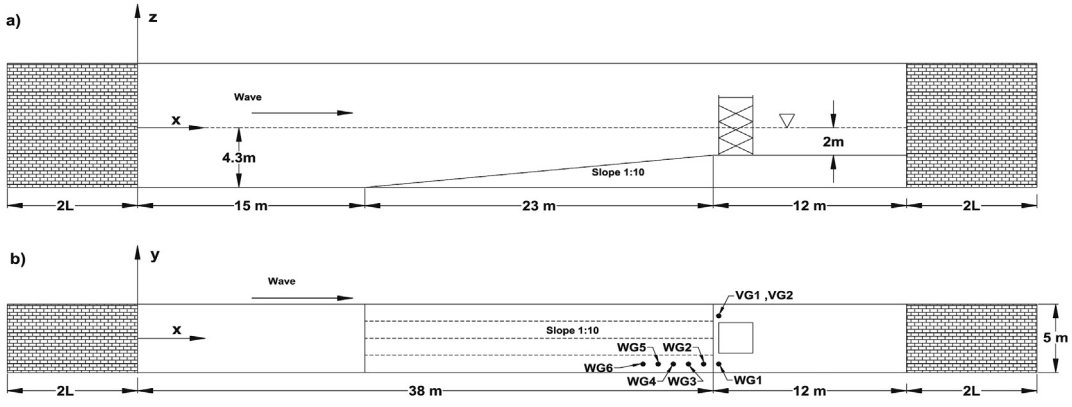

Fig. 4. Schematic representation of Numerical Wave tank (Jose et al., 2016a). a) Cross section, b) Plane view.

Table 2
Grid configurations.

G1	G2
0.04 m × 0.03 m × 0.03 m	0.03 m × 0.03 m × 0.03 m

members of the jacket structure. Table 1 shows 13 incident wave conditions (one non-breaking case and 12 breaking cases) considered in the present research. Each of these test cases is studied in detail in terms of breaking wave shapes, wave breaking points, total breaking wave forces on the jacket structure and breaking wave forces on the local members of the jacket structure. Moreover, the variation in the slamming coefficients along the length of the local members is discussed.

A grid sensitivity study is carried out on the numerical model before performing the simulations. The simulations were performed for two different grid configurations as shown in Table 2. Fig. 5 shows the wave surface elevation and total wave forces on the structure for the two different grid configurations, G1 and G2. The grid configuration G1 is comparatively coarser than G2. It is observed that the there is no significant difference in the results for both grid configurations. However, in the present simulations a finer grid (G2) is used to calculate the wave forces on the structure. In the NWT, the grid size varied from a minimum of 0.03 × 0.03 × 0.04 m near the jacket structure to a maximum of 0.3 × 0.2 × 0.4 m far from the structure.

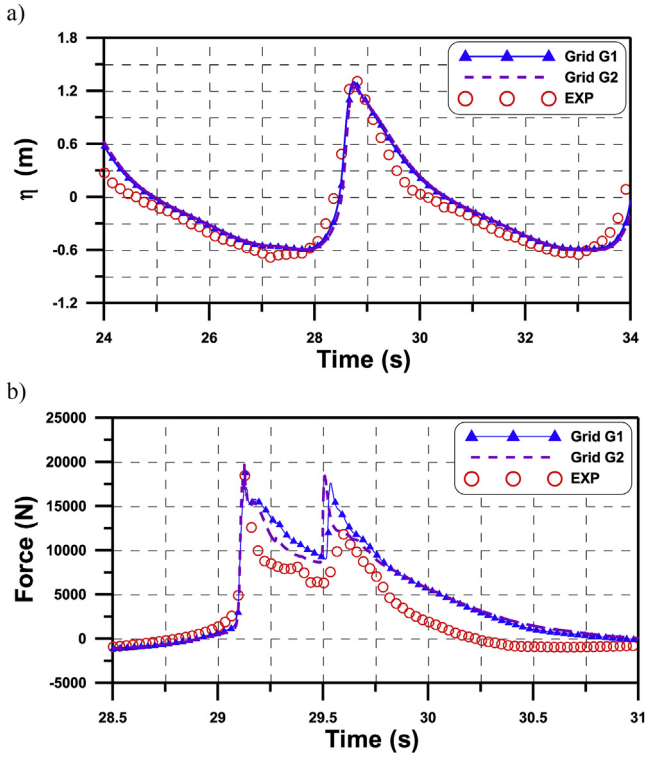

Fig. 5. Comparison of the wave surface elevations and total force on the structure using two different grid configurations for the wave case b3. a) Wave surface elevation at wave gauge WG4 using grid configuration G1 and G2. b) Total force on the jacket structure using grid configurations G1 and G2.

3.1. Wave surface elevation

As the wave breaking is very sensitive to the wave height, it is important to accurately simulate the exact wave height in the numerical model. The free surface elevation calculated by the numerical model is validated against the experimental data for all the wave cases presented in Table 1. As all the wave gauges used in the experiment were resistance type wave gauges, we cannot expect a reliable measurement after the breaking point due to the curling of the wave and entrained air bubbles in the wave breaker. Hence, in all test cases the comparison of free surface elevation between the CFD results and the measured results are performed for the wave gauges, which are just before the wave breaking.

Fig. 6 shows the comparison of free surface elevation for the non-breaking wave case at the wave gauges WG1 and WG2. In the case of the non-breaking wave (see Fig. 6), the numerical calculations shows exact agreement with the experimental measurements. The nonlinearity in the wave is not much predominant in this case.

Figs. 7 and 8 show the comparison between the calculated and the measured free surface elevation at WG4, WG5, and WG6, for cases b3 and d2. Overall, the calculated results agree reasonable well with the experimental measurements for all the simulated cases. Especially, for case d2, the peaks at both the wave crest and trough are reproduced very well in the numerical results. However, for case b3, the calculated results

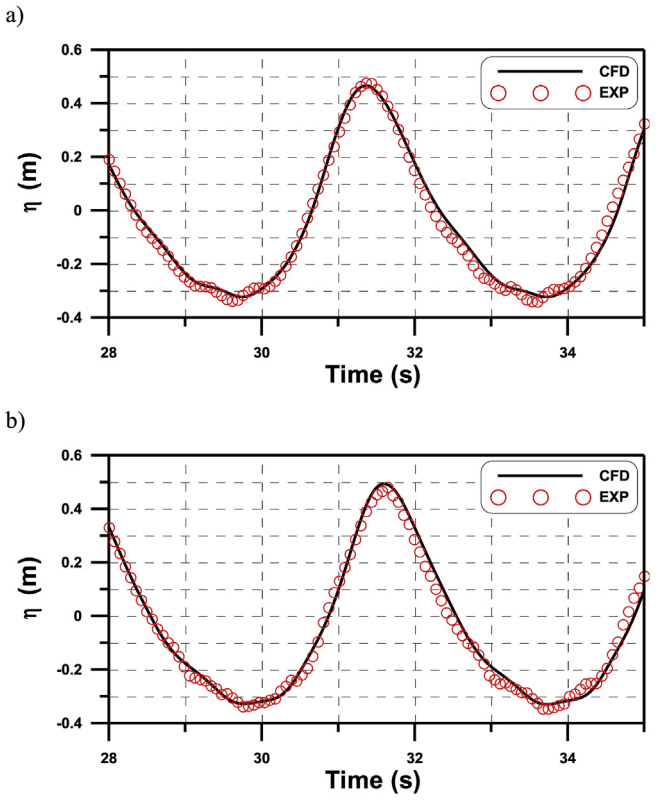

Fig. 6. Comparison of the free surface elevations between the CFD results and experimental results for case a1 (Jose et al., 2016a). (a) Wave gauge WG2 and (b) Wave gauge WG1.

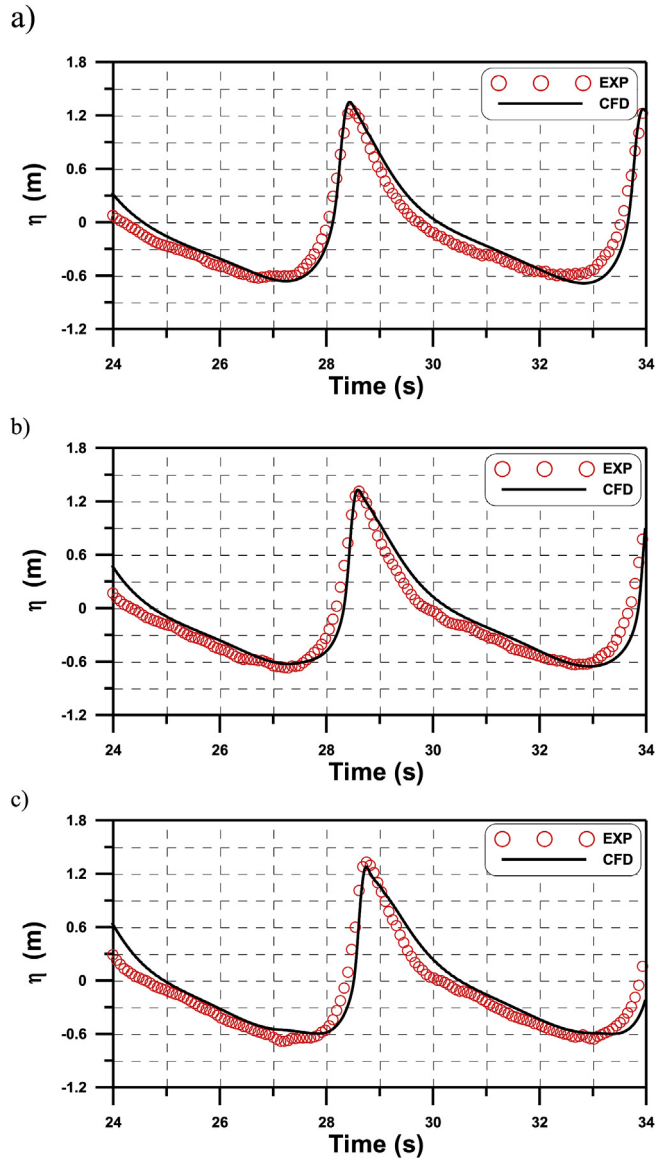

Fig. 7. Comparison of the free surface elevations between the CFD and experimental results for case b3. (a) Wave gauge WG6; (b) Wave gauge WG5 and (c) Wave gauge WG4.

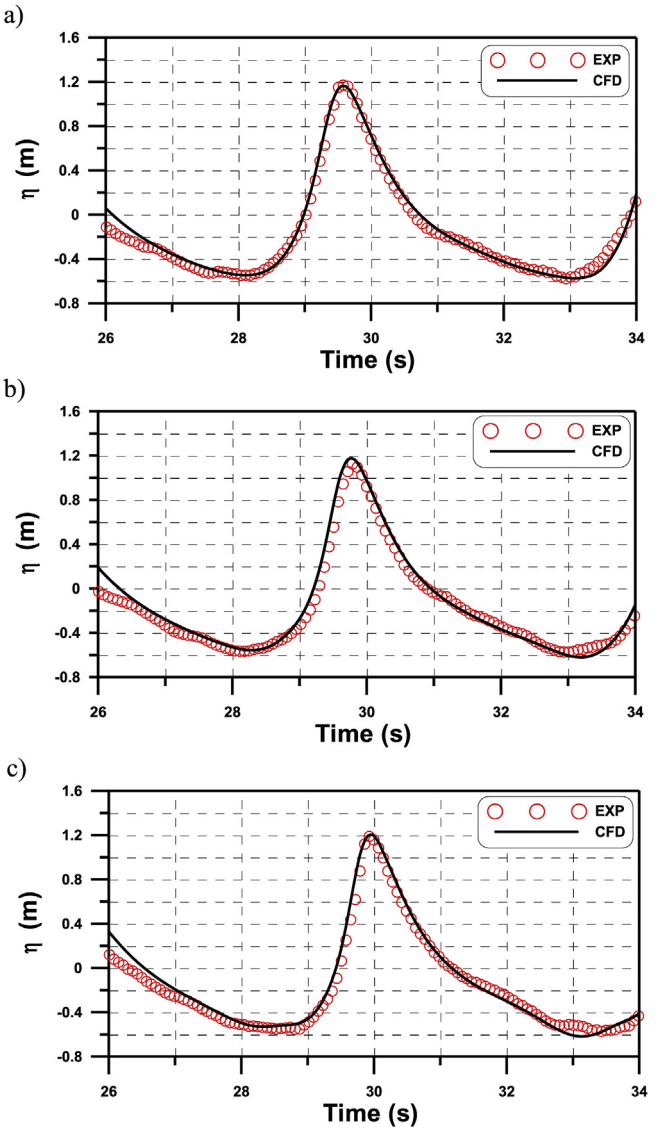

Fig. 8. Comparison of the free surface elevations between the CFD and experimental results for case d2.(a) Wave gauge WG5; (b) Wave gauge WG4 and (c) Wave gauge WG3.

on the fall-time are slightly overestimated compared with the measured results. Meanwhile, it should be noted that even though the results for other cases are not presented in the paper, the calculated results also show a reasonable agreement with the measured data. The snapshots of the spatiotemporal variations of the instantaneous water level for case b3 are shown in Fig. 9.

3.2. Water particle velocities

In the experiment, three Acoustic Doppler Velocity (ADV) meters were used to measure the water particle velocities. However, the ADV meter near the SWL didn't accurately register measurements due to air pockets in the wave breaker. Moreover, some noises are observed in the measurements for strong breaking wave cases.

Figs. 10 and 11 show the comparison of water particle velocities between the measured data and CFD results, for cases b3 and d2, respectively. The velocities calculated by the Navier–Stokes solver agree reasonably well with the measured velocities. There is a good agreement in peak velocities with the experimental and numerical results. The slight discrepancies observed would be due to the disturbances in the measuring equipment due to the high turbulence during the wave breaking. Moreover, the experimental measurements look noisy compared to numerical results.

3.3. Total breaking wave forces

In the experiment, the total breaking wave forces on the jacket structure were measured using four total force transducers integrated with the jacket structure. The measured force

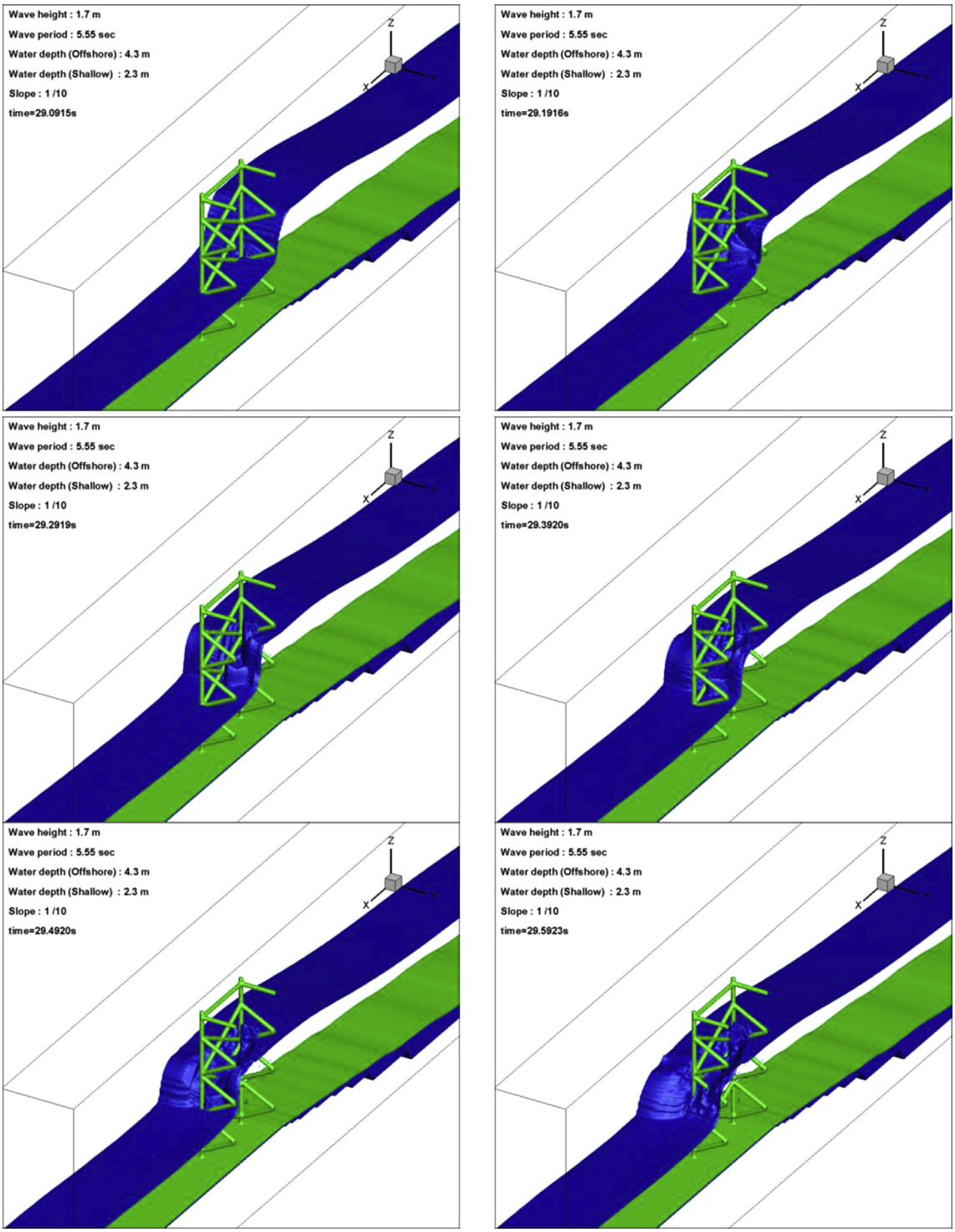

Fig. 9. Snapshots of the spatiotemporal variations of instantaneous water level for case b3 (time = 29.0915 s, 29.1916 s, 29.2919 s, 29.3920 s, 29.4920 s and 29.5923 s).

responses contain the quasi-static forces, the net breaking wave forces and the amplified force component due to structure's vibration. On the other hand, in the numerical model, the jacket structure is modelled as completely rigid structure which cannot induce dynamic amplification due to the structure's vibration. Therefore, in order to make quantitative comparison between the CFD results and experimental data, the amplified forces component due to structure's vibration in the measured force responses should be removed with the help of the EMD method as explained by Jose et al. (2016a), and then the filtered results are compared with the CFD results.

Fig. 12 shows the total wave forces on the structure for the non-breaking case a1. There is no dynamic amplification in the measured response forces, hence a direct comparison of the

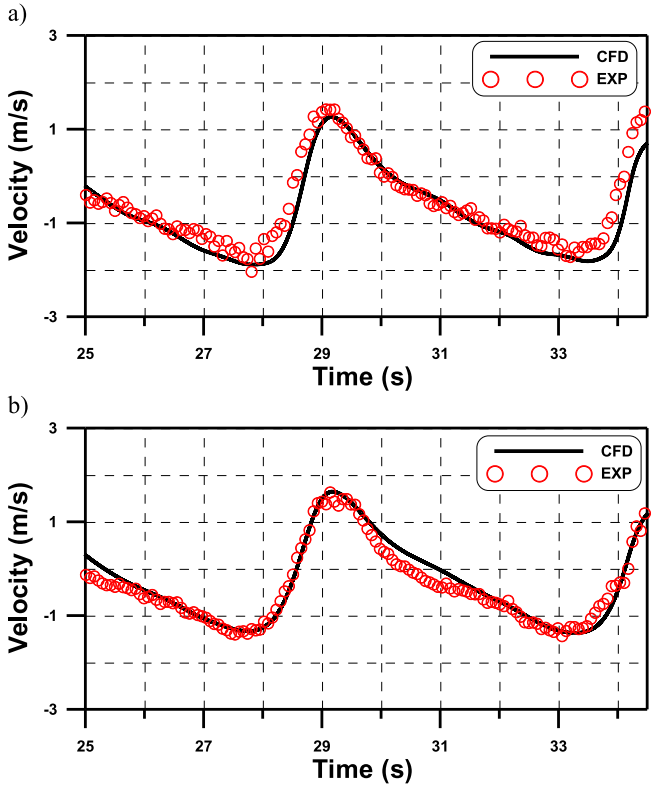

Fig. 10. Comparison of the water particle velocities between the CFD and experimental results for case b3. (a) Velocity gauge VG1 and (b) Velocity gauge VG2.

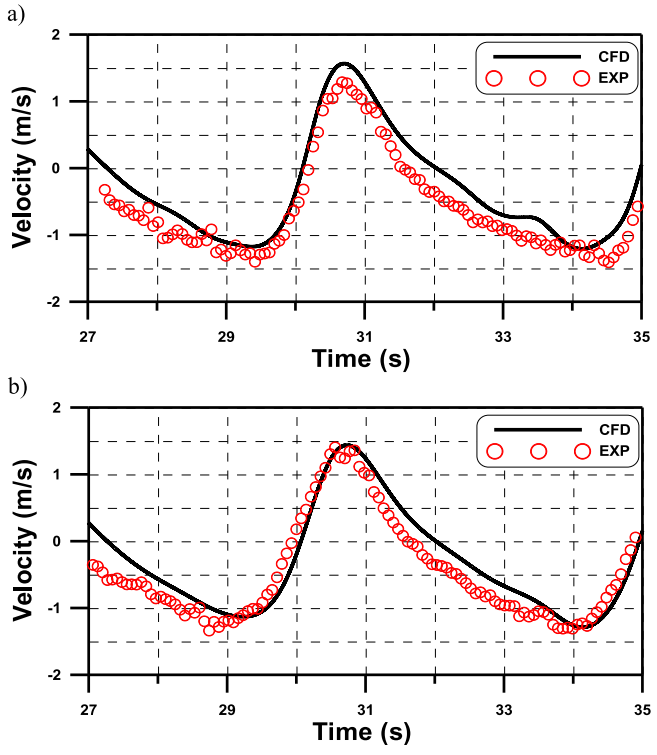

Fig. 11. Comparison of the water particle velocities between the CFD and experimental results for case d2. (a) Velocity gauge VG1 and (b) Velocity gauge VG2.

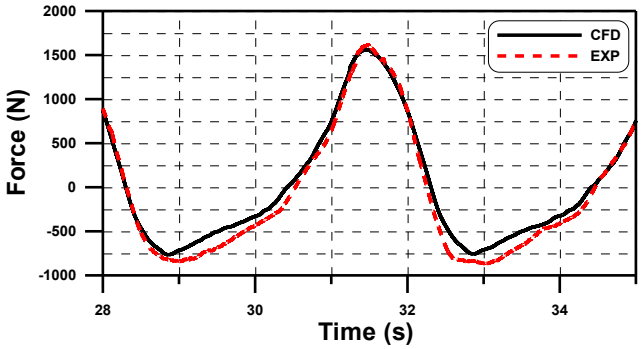

Fig. 12. Comparison of total wave force on the structure between the CFD and experimental results for non-breaking case a1.

measured total force and the numerical calculation is done. The total force is similar to the quasi-static Morison force. The CFD results show very good agreement with the experimental results. Figs. 13–16 show the comparison of filtered breaking wave forces (EXP) and breaking wave forces computed by the CFD model for difference wave cases. For the breaking waves, in the total force time series there are two different peaks, which represent the wave impacts on front and back side of the jacket structure. Based on the initial observation of the total force time series, it is observed that for higher periods and wave heights, the forces on the jacket structure are high. In all the wave cases with wave height 1.5 m, the wave breaking occurs beyond the front of the jacket structure. The higher second peak in the total force time series is observed for these wave cases (b1, c1, d1 and e1). For the other wave cases, in most of the time the wave breaks ahead of the structure. However, the total forces depend on many other parameters such as wave breaking position, wave height, wave period, etc.

In the total force comparison, the first peak in the CFD model shows very good agreement with the experimental data, however, the second peak is slightly overestimated. As explained by Jose et al. (2016a), there are many reasons attribute to this difference in the force. Firstly, in the experimental measurements, when the wave breaks on the structure there are lot of entrained air bubbles in the wave breaker. The presence of these air bubbles in the wave breaker reduces the effective density of the water hitting the structure and hence reduces the forces on the structure. Similar observations are made by several researchers based on experimental and numerical studies (Choi et al., 2015; Hu and Kashiwagi, 2004; Obhrai et al., 2004; Tang and Wai, 2016; Hoque, 2002). However, in the present numerical model, these kinds of effects cannot be simulated due to the use of incompressible flow model. The absence of entrained air bubbles in the wave breaker (in incompressible model) reduces the energy dissipation by 20–25% (Hoque, 2002). This reduced energy dissipation would cause larger energy in wave breaker even after the wave breaking is initiated. Secondly, the unsymmetrical wave breaking on the jacket structure will introduce difference in the experimental measurements. It was observed in the experimental measurements that the wave is not hitting the structure symmetrical always, i.e., the breaking wave front is not exactly

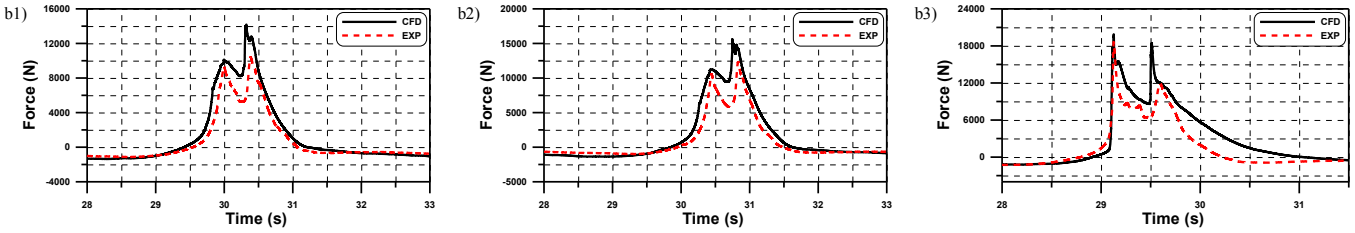

Fig. 13. Comparison of total wave force on the structure between the CFD and experimental results for breaking cases b1–b3.

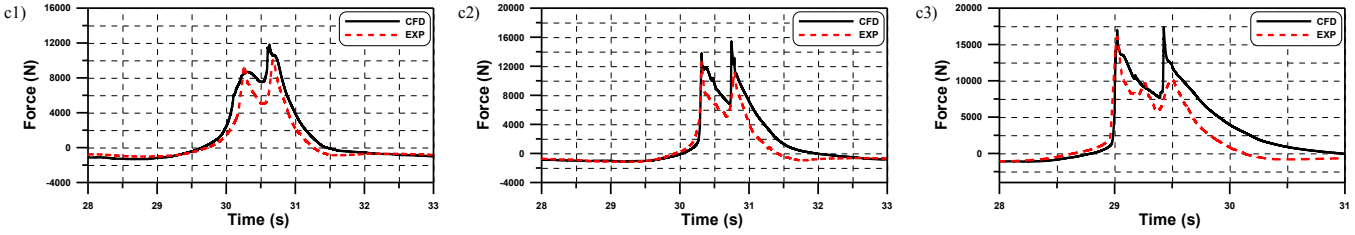

Fig. 14. Comparison of total wave force on the structure between the CFD and experimental results for breaking cases c1, c2 (Jose et al., 2016a) and c3.

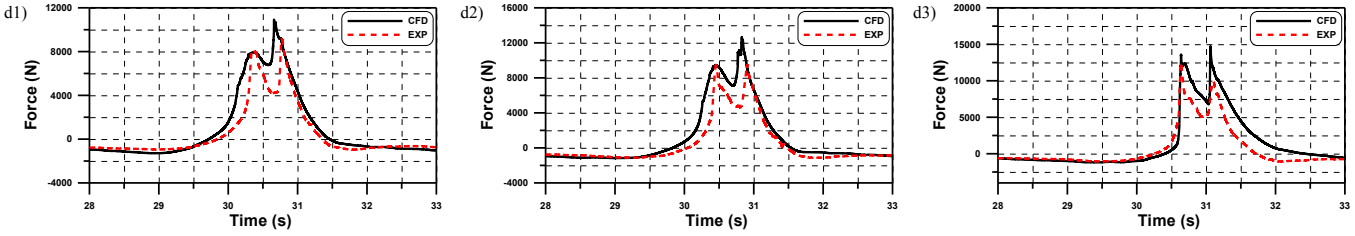

Fig. 15. Comparison of total wave force on the structure between the CFD and experimental results for breaking cases d1–d3.

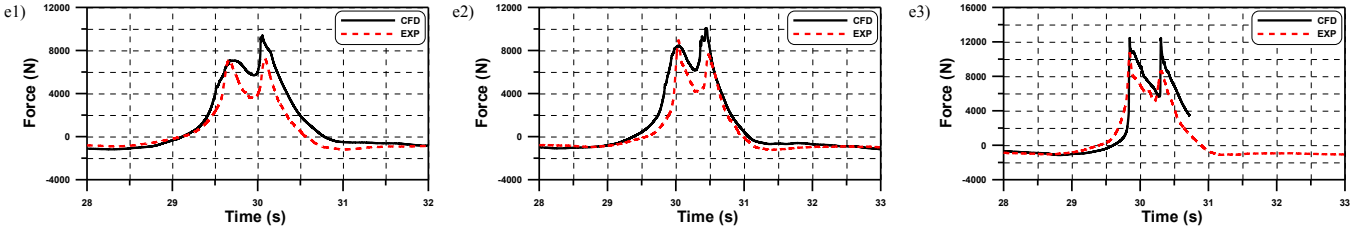

Fig. 16. Comparison of total wave force on the structure between the CFD and experimental results for breaking cases e1–e3.

parallel to the jacket structure always. Even though the degree of asymmetry is in terms of milliseconds, it has a larger impact on the total forces on the structure. These kinds of unsymmetrical wave impact cannot be simulated by the present CFD model. Thirdly, in the CFD model, the jacket structure is modelled taking into account x-axis symmetry. The total forces on the jacket structure are calculated by multiplying the forces on half structure with a factor of 2. However, in the experimental measurements it was observed that the wave interactions on the left and right side of the structure is slightly different. Finally, in the present numerical model the wave breaking is slightly slower compared to the experimental measurements in terms of energy dissipation. The absence of entrained air bubbles in the breaker would result shift in the wave breaking position (Hoque, 2002). Despite the discrepancies, the overall results show a reasonable agreement with experimental data. Therefore, it is concluded that the proposed numerical model can be used to predict the slamming coefficients on local members of a jacket structure.

4. Calculation of slamming coefficients

Based on the validated numerical results, the slamming coefficients for the members B1 (front upper inclined member), B2 (front lower inclined member), B3 (back upper inclined member), B4 (back lower inclined member), B5 (side-downward member), B6 (side-upward member), V1 (front vertical member) and V2 (back vertical member) of the jacket structure are obtained. The slamming coefficients on the members are calculated as discussed in the section 2.4.

Figs. 17–24 show the variation of maximum slamming coefficients along the length of the members for different wave conditions shown in Table 1. It is evident that the distribution of slamming forces on the structure depends greatly on the breaking wave conditions. For example, if the wave breaks too far from the structure, broken waves will reach the structure and the breaking wave forces will be less and more spread. One the other hand, if the wave breaks in front of the structure, very high breaking wave forces will act on the structure. As in the present cases the water depth is fixed, the wave height and wave period decides the intensity of wave breaking forces on the structural members. Hence, a detailed comparison of slamming coefficients for different combinations of wave height and period are carried out in this section.

4.1. Vertical member V1

Fig. 17 shows the variation in the slamming coefficients on the front-vertical member of the jacket structure V1. A triangular distribution of slamming coefficient is observed for all the cases, unlike the distribution presented by Goda et al. (1966) and Wienke and Oumeraci (2005). Looking at Fig. 17a, for the wave height 1.5 m case, the slamming coefficient variation looks similar for different wave periods. Since the wave breaks in between the structure (weakly breaking case at the front vertical member), the slamming coefficients obtained are found to be similar to drag coefficient. For 1.6 m case (Fig. 17b), the wave breaking points are shifted more to the front vertical member. Hence, the wave breaking is stronger than the 1.5 m case. The maximum slamming coefficient for the 1.6 m case is obtained for the wave period 5.2 s (Fig. 17b) due to the breaking of wave near the front members of the jacket structure. In the case of wave height 1.7 m (Fig. 17c), the wave breaking point is in front of the structure causing larger wave forces to act on the front member. The distribution of slamming coefficients along the vertical member becomes steeper as the wave periods decrease (from 5.55 s to 4.6 s). Especially, for case e3 (H = 1.7 m and T = 4.6 s), because of the high wave steepness the breaking wave forces on the front-vertical member become less spread and result in higher slamming coefficient compared to the other cases. The maximum slamming coefficient obtained for the vertical member V1 is 2.96.

4.2. Vertical member V2

Fig. 18 shows the variation in the slamming coefficient on the back-vertical member of the jacket structure, V2. A triangular distribution of slamming coefficient is observed for all the cases. For the cases with wave height 1.5 m (Fig. 18a), since the waves break beyond the front of the structure, the higher wave forces are observed at the back vertical member. The slamming coefficients increase as the wave period decrease from 5.55 s to 4.9 s due to the shifting of the wave breaking position from the back side of the structure to the front of the back members. Maximum slamming coefficient for the vertical member V2 is observed for the wave period 4.9 s. For wave height 1.6 m case (Fig. 18b), the slamming coefficients are still high at the back vertical member. The positions of maximum slamming coefficients are slightly lower than the positions for the wave height 1.5 m case due to the shifted wave breaking point. Meanwhile, for 1.7 m cases (Fig. 18c), broken wave reaches the back members and hence the distribution of slamming force is more spread and less impulsive. The maximum slamming coefficient obtained for the vertical member V2 is 2.63.

4.3. Bracing member B2

Fig. 19 shows the variation in the slamming coefficients on the front-lower bracing of the jacket structure, B2. The distribution of slamming coefficient is found to be more uniform (like rectangular type) along the bracing member. The results imply that the breaking wave impacts the member like a vertical wall of water. In some details, for the wave case b3

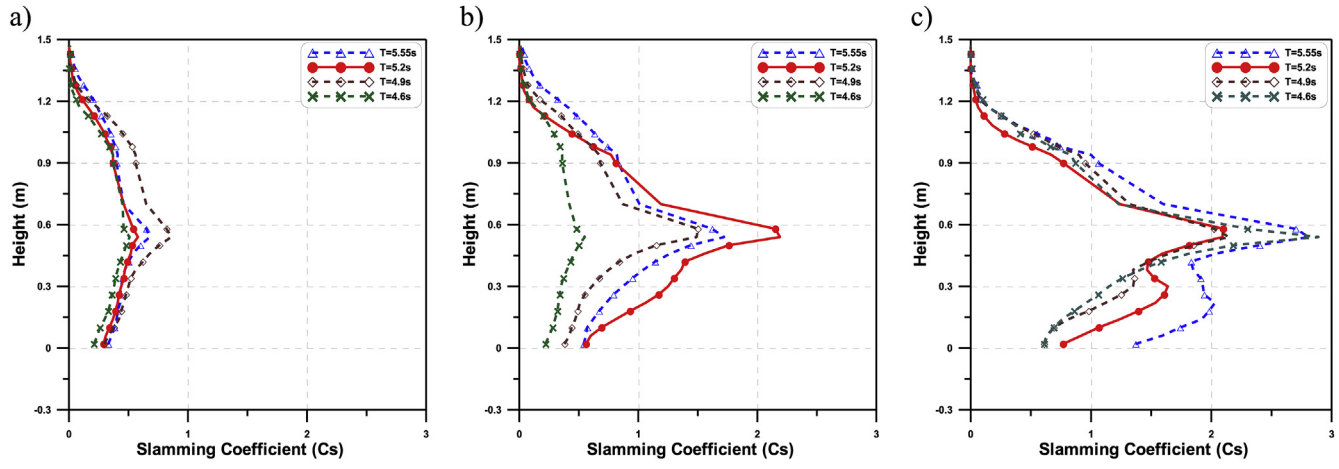

Fig. 17. Comparison of maximum slamming coefficient along the length of the vertical member V1 of the jacket structure for a) H = 1.5 m (b1, c1, d1 and e1), b) H = 1.6 m (b2, c2, d2 and e2), c) H = 1.7 m (b3, c3, d3 and e3).

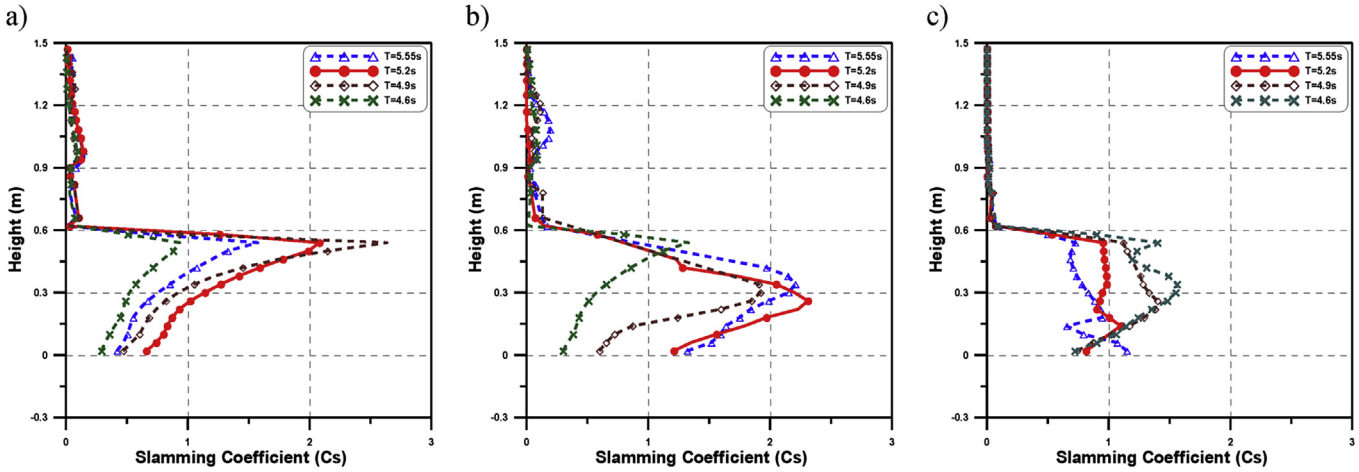

Fig. 18. Comparison of maximum slamming coefficient along the length of the vertical member V2 of the jacket structure for a) H = 1.5 m (b1, c1, d1 and e1), b) H = 1.6 m (b2, c2, d2 and e2), c) H = 1.7 m (b3, c3, d3 and e3).

(H = 1.7 m, T = 5.55 s), the variation in the slamming coefficient on the member is fluctuating compared with other cases. This can be attributed to the violent breaking of the wave on the structure member. Looking at Fig. 19a, the slamming coefficients for various wave cases look similar. In all these cases the breaking of the wave is beyond the front members of the jacket structure. On the other hand, Fig. 19b, due to the shifting of the wave breaking position toward the front of the jacket structure with the decrease in the wave period, higher slamming coefficients are obtained for c2 (H = 1.6 m, T = 5.2 s). The maximum slamming coefficient for the bracing member B2 is obtained for wave case e3 (H = 1.7 m, T = 5.55 s) and the value is 7.87. This value is slightly higher than the slamming coefficient suggested by Wienke and Oumeraci (2005). However, this higher value of slamming coefficient is obtained very local to the bracing member. When we compare the distribution of slamming coefficient on the upper bracing member (B1) and lower bracing member (B2), the slamming coefficient is triangular type for the upper member and nearly rectangular type for the lower member. This is agrees with the physical representation of the breaking wave that the upper part of the breaker is curled and lower part is more like a vertical wall of water. This also indicates that the distribution of slamming forces on the member depends directly on the shape of the wave front hitting the structure.

4.4. Bracing member B4

Fig. 20 shows the variation in the slamming coefficient on the back-lower bracing of the jacket structure, B4. In contrast with the front lower bracing member B2, the distribution of slamming coefficient is more triangular. When the wave reaches the back members, the 'wall of water' impact effect is absent due to the overturning of the wave after breaking. Hence a triangular distribution of slamming coefficient is observed, especially for wave height 1.7 m (Fig. 20c). In the case of wave height 1.5 m cases (Fig. 20a), the wave breaking

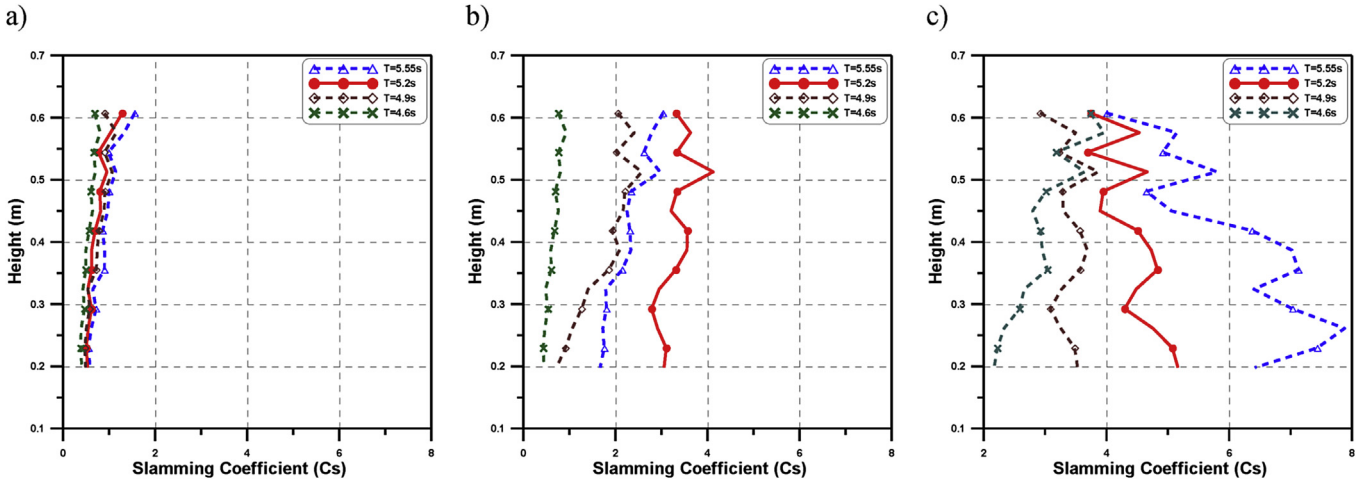

Fig. 19. Comparison of maximum slamming coefficient along the length of the bracing member B2 of the jacket structure for a) H = 1.5 m (b1, c1, d1 and e1), b) H = 1.6 m (b2, c2, d2 and e2), c) H = 1.7 m (b3, c3, d3 and e3).

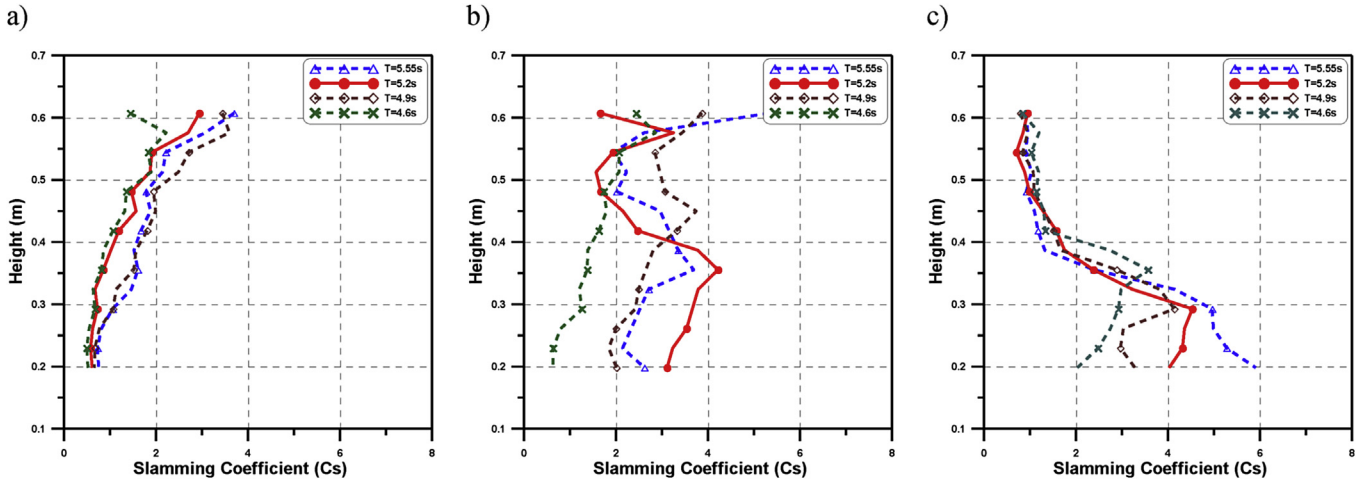

Fig. 20. Comparison of maximum slamming coefficient along the length of the bracing member B4 of the jacket structure for a) H = 1.5 m (b1, c1, d1 and e1), b) H = 1.6 m (b2, c2, d2 and e2), c) H = 1.7 m (b3, c3, d3 and e3).

take place near the back of the jacket structure. Hence a uniform distribution of slamming coefficient is observed for the back bracing members. The maximum slamming coefficient obtained for the bracing member B4 is 5.90.

4.5. Bracing member B1

Fig. 21 shows the variation of maximum slamming coefficients along the length of the front upper bracing member, B1. The maximum slamming coefficients are observed at the bottom elevation of the member. A linear variation in the slamming coefficient is observed for various wave cases. Looking at Fig. 21a, for the wave height 1.5 m the slamming coefficient looks very small due to the weakly breaking wave near the front members. However the for 1.6 m (Fig. 21b) and 1.7 m (Fig. 21c), the wave breaking is more on to the front members, hence higher the slamming coefficients. The maximum slamming coefficient is observed for the wave case b3 (H = 1.7 m, T = 5.55 s), where the wave breaks just ahead of the structure. The maximum slamming coefficient calculated was 2.4.

4.6. Bracing member B3

Fig. 22 shows the variation in the slamming coefficient on the back-upper bracing of the jacket structure, B3. Unlike the results for the front upper bracing B1, the variation of slamming coefficient along the bracing member follows different pattern depending on the wave breaking conditions. Looking at Fig. 22c, for the wave height 1.7 m cases, the slamming coefficient for the back upper bracing member is small compared to 1.5 m (Fig. 22a) and 1.6 m (Fig. 22b) wave cases. This is due to the less intense wave reaching the upper bracing members for 1.7 m case. However, for 1.6 m and 1.5 m cases, a triangular distribution of slamming coefficient is observed for shorter wave periods, due to the breaking of the waves on the back members. The maximum slamming coefficient obtained for the bracing member B3 is 3.06.

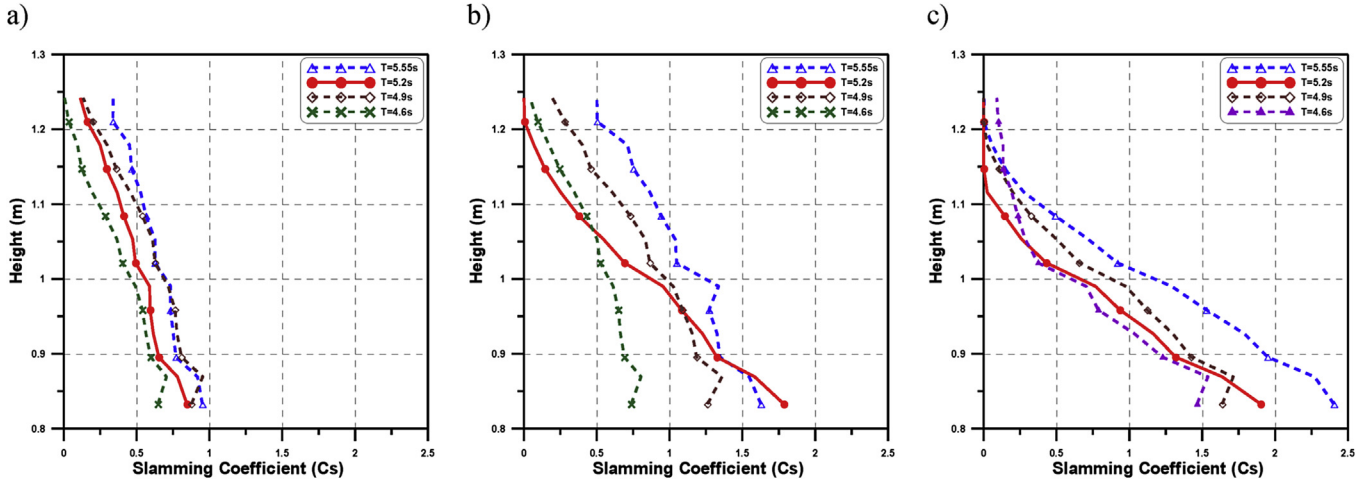

Fig. 21. Comparison of maximum slamming coefficient along the length of the bracing member B1 of the jacket structure for a) H = 1.5 m (b1, c1, d1 and e1), b) H = 1.6 m (b2, c2, d2 and e2), c) H = 1.7 m (b3, c3, d3 and e3).

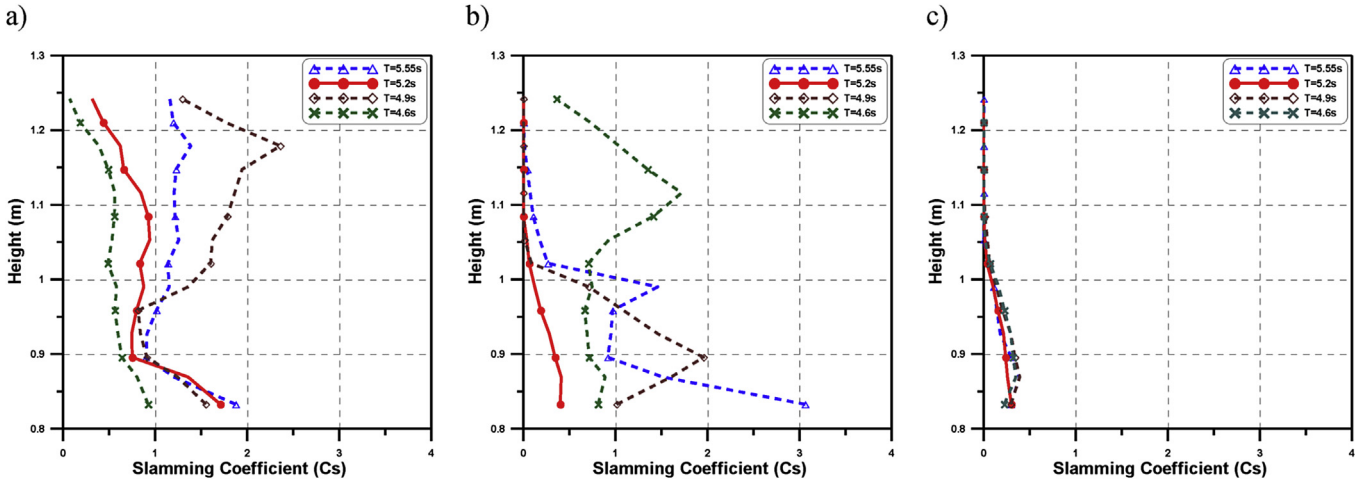

Fig. 22. Comparison of maximum slamming coefficient along the length of the bracing member B3 of the jacket structure for a) H = 1.5 m (b1, c1, d1 and e1), b) H = 1.6 m (b2, c2, d2 and e2), c) H = 1.7 m (b3, c3, d3 and e3).

4.7. Bracing member B5

Fig. 23 shows the variation in the slamming coefficient for the side-downward bracing of the jacket structure B5. Based on the video recordings from the experiment and simulations, it was evident that the slamming forces on the side members are shaded by the front vertical members. However, due to the encounter of the waves which are generated at the left and right sides of the front vertical member, high wave forces are observed in the middle of the member B5. This effect diminishes with the distance from the front member, which results on larger forces near the middle length of the bracing member as shown in Fig. 23a and b. For 1.7 m (Fig. 23c), due to the strong plunging breaker, the encounter of the waves are not predominant and hence the forces increases almost linearly with the distance from the front vertical member. The maximum slamming coefficient obtained for the bracing member B5 is 1.00, which is similar to the drag coefficient. It is expected that the slamming forces on these members will become critical if the wave impacts the structure in oblique direction.

4.8. Bracing member B6

Fig. 24 shows the variation in the slamming coefficient for the side-upward bracing (B6) of the jacket structure. For the wave height 1.7 m case (Fig. 24c), the broken wave is reaching the member and the computed forces are small. However, for 1.5 m (Fig. 24a) cases, the force is larger as the wave is breaking near the back members. The shading effect of the front vertical member V1 is not obvious in this case as the member is far from the vertical member. The maximum slamming is observed near the upper elevation of the bracing member. The maximum slamming coefficient obtained for the bracing member B5 is 1.45.

4.9. Discussion on slamming coefficients

In earlier studies on monopile structures (Wienke and Oumeraci, 2005), the slamming coefficients were determined only for cases where the wave breaks in front of structure. However, compared to monopile, a jacket structure is more

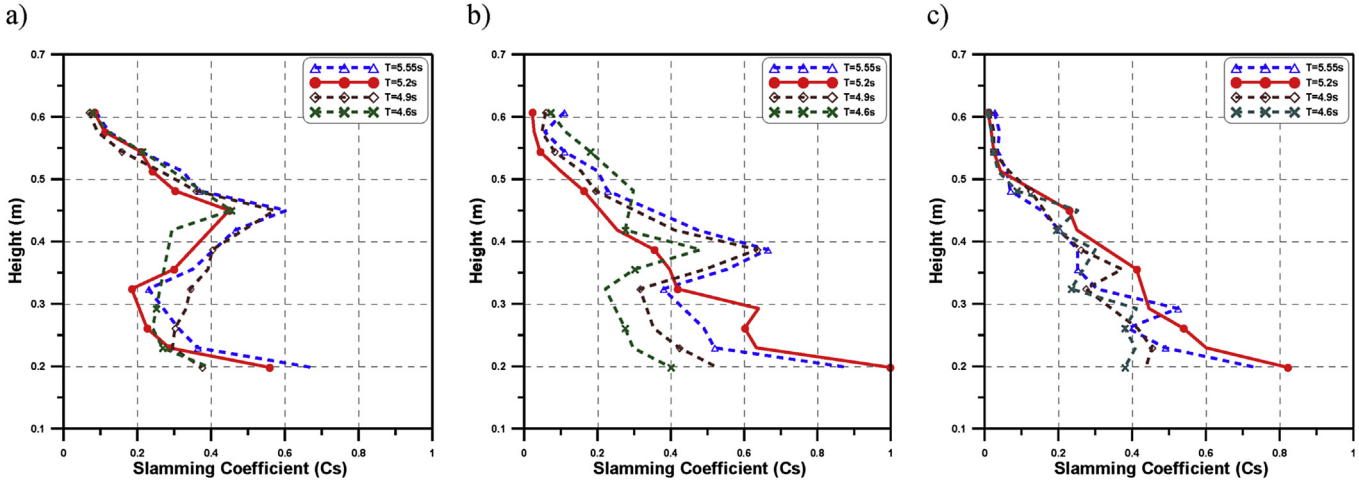

Fig. 23. Comparison of maximum slamming coefficient along the length of the bracing member B5 of the jacket structure for a) H = 1.5 m (b1, c1, d1 and e1), b) H = 1.6 m (b2, c2, d2 and e2), c) H = 1.7 m (b3, c3, d3 and e3).

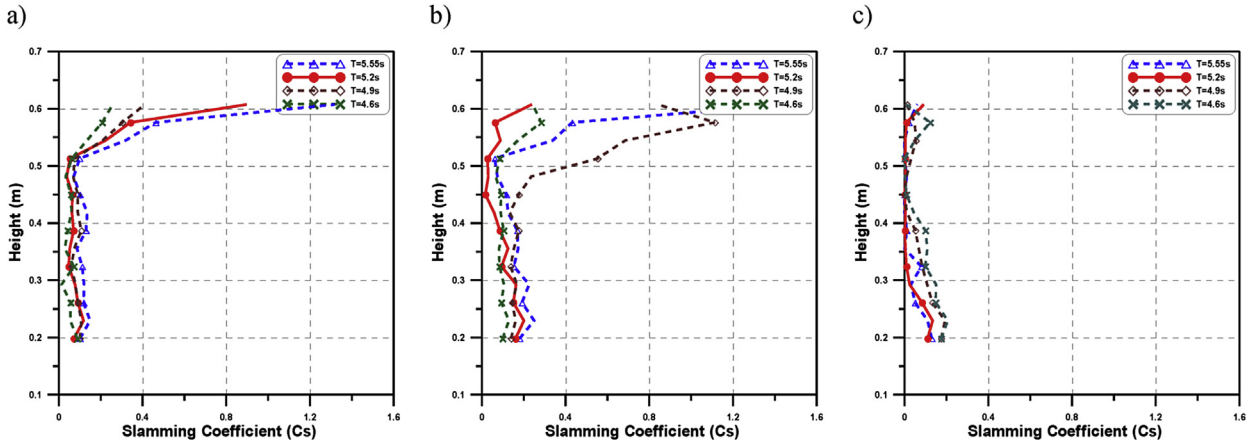

Fig. 24. Comparison of maximum slamming coefficient along the length of the bracing member B6 of the jacket structure for a) H = 1.5 m (b1, c1, d1 and e1), b) H = 1.6 m (b2, c2, d2 and e2), c) H = 1.7 m (b3, c3, d3 and e3).

complex having more structural members. It is therefore important to investigate the effect of wave breaking positions relative to the structure on the local member forces. A number of breaking wave cases are simulated in present study and conclusions are drawn.

It is found that the wave breaks at different positions relative to the jacket structure depending upon the wave height and the wave period. The strong breaking waves are represented by the cases where wave breaks in front of the structure. These cases are simulated by a wave height of 1.7 m and 1.6 m and the maximum slamming coefficients are estimated on the front members of the jacket structure. It is also observed that the wave breaking position shifts slightly ahead of the structure as the wave period decreases. This reduces the slamming forces on the structure members and a range of slamming coefficients is expected for the jacket members depending on the wave breaking positions. For the front upper bracing member, a maximum slamming coefficient is found in the range 0.80–2.40 for the cases where wave breaks in front of the structure. The smaller values of slamming coefficients are estimated for the shorter waves due to early breaking of the wave. For the back upper bracing members, the slamming coefficients are found to be smaller than the drag coefficients due to broken waves reaching the members. However, for the same wave breaking positions, the slamming coefficients are found to be higher for the lower bracing members. The coefficients are in range of 0.93–7.87 and 2.86 to 5.90 for front and back lower bracing members respectively. A similar trend is observed for front vertical members where the slamming coefficients are in range of 0.55–2.96. For back vertical members, the coefficients are close to the drag coefficients. It is observed that as the distance from the members of the structure and the breaking point increases, the slamming coefficient decreases. Also, the forces on the back members are lower than the front members in all these cases.

For weakly breaking waves, the wave breaking position further shift beyond the front of the structure. These cases are represented by a wave height of 1.5 m and some of the cases with 1.6 m wave height, in the present simulations. Among these cases, the 1.6 m cases are found more critical resulting in higher slamming force on the jacket members. However, the slamming coefficients are found to be lower than the cases where the wave breaks in front of the structure. The maximum wave breaking forces are observed for the back members due to wave breaking beyond the front of the jacket structure. For the back lower bracing, the maximum slamming coefficient is found to be in the range of 2.22–5.33. The lower values correspond to the cases where the wave breaks far from the back member. The slamming coefficient for the front lower and back upper bracing members is in range of 0.81–3.03 and 0.92 to 3.06 respectively. In addition, smaller values of the slamming coefficient are observed for the front upper bracings. The range of slamming coefficients for the back vertical members is 0.93–2.63 and for the front vertical member is 0.51–1.72. Table 3 summarized the values of maximum slamming coefficients calculated for different members of jacket structure in the wave impact zone.

Table 3
Summary of maximum slamming coefficients for different wave cases (maximum slamming coefficient for each member is shown).

Wave case	Slamming coefficient, C_s								Breaking position
	B1	B2	B3	B4	B5	B6	V1	V2	
b1	0.95	1.55	1.88	3.70	0.67	1.32	0.68	1.57	Behind the back leg
b2	1.63	3.03	3.06	5.33	0.88	1.45	1.72	2.21	Middle of the structure
b3	2.40	7.87	0.39	5.90	0.74	0.13	2.81	1.15	In front of front leg
c1	0.85	1.29	1.71	2.96	0.56	0.90	0.58	2.08	At the back leg
c2	1.79	4.12	0.41	4.22	1.00	0.24	2.19	2.31	In front of front leg
c3	1.90	5.17	0.30	4.53	0.82	0.13	2.09	1.10	In front of front leg
d1	0.95	1.16	2.36	3.59	0.57	0.41	0.86	2.63	In front of back leg
d2	1.36	2.58	1.96	3.87	0.64	1.11	1.50	1.92	In front of front leg
d3	1.71	3.87	0.39	4.13	0.45	0.19	2.15	1.40	In front of front leg
e1	0.70	0.81	0.92	2.22	0.45	0.26	0.51	0.93	Middle of the structure
e2	0.80	0.93	1.72	2.86	0.48	0.28	0.55	1.33	In front of front leg
e3	1.24	3.96	1.24	3.57	0.41	0.21	2.94	1.56	In front of front leg

5. Conclusions

A comprehensive study on breaking wave interaction on a jacket structure is performed by simulating wide range of breaking wave conditions in the NWT. The wave surface elevation, water particle velocities and the breaking wave forces on the jacket structure are computed by the 3D numerical model and the computed results show a good agreement with the experimental measurements. However, slight discrepancies are observed due to the use of incompressible flow model used in the present simulations.

The local breaking wave forces on the members of the jacket structure were calculated by the force transducers distributed along the jacket members. The maximum forces calculated by each of these local force transduces were used to estimate the corresponding local maximum slamming coefficients. Further, the distribution of maximum slamming coefficients along the length of the jacket members is obtained. The distribution of slamming forces on the local members in impact area are triangular shape, unlike the research by Goda et al. (1966) and Wienke and Oumeraci (2005) (In their research, breaking wave forces are evenly distributed along the impact area). This discrepancy can cause different response characteristics of entire (or local) structure. Therefore, the use of accurate distribution is of great importance in the design of OWT substructure.

In the present study a wide range of wave breaking cases are taken into account, from weakly breaking to strongly breaking wave cases. The maximum slamming coefficients are estimated for the front members of the jacket structure, when the wave breaks in front of the structure. Based on the present simulations, the maximum slamming coefficient for the bracing members of the jacket structure in the wave impact zone is estimated as 7.87, which is similar to the value suggested by Wienke and Oumeraci (2005). On the other hand, in the case of vertical member, maximum slamming coefficient is obtained to be 2.96, which is slightly smaller than the values suggested by Goda et al. (1966). However, in the design of OWT substructures, it is not advised to use the maximum value of slamming coefficient along the entire member. A triangular distribution of force should be adopted in the calculation of slamming forces on the members.

The limitations of the present study are also identified. One of the limitations is the use of numerical model based on incompressible flow. As a result, the presence of entrained air bubbles in the breaker is not considered in the present simulations. It is reported that the absence of entrained air bubbles in the simulation have some influence on the wave breaking position and the forces on the structure (Hoque, 2002). Further studies are needed to verify the proposed slamming coefficients for the jacket structure and also to investigate the effect of air bubbles on these values.

Acknowledgements

This research was supported by NORCOWE (Project No: PR-10077) and University of Stavanger. The authors would like to thank Professor. Ove Tobias Gudmestad (UiS) for his critical review of the paper and comments. The AP-AMG solver for solving the Poisson Pressure Equation was provided by Chihiro Iwamura, Allied Engineering Corporation, Japan.

References

Alagan Chella, M., Bihs, H., Myrhaug, D., Muskulus, M., 2016. Breaking solitary waves and breaking wave forces on a vertically mounted slender cylinder over an impermeable sloping seabed. J. Ocean Eng. Mar. Energy 1–19.

Allied Engineering, 2011. User's Manual for Advanced Parallel AMG Version 1.3. Tokyo.

Amsden, A.A., Harlow, F.H., 1970. A simplified MAC technique for incompressible fluid flow calculation. J. Comput. Phys. 6, 322–325.

Arntsen, Ø.A., Gudmestad, O.T., 2014. Wave slamming forces on truss structures in shallow water. In: Proceedings of the HYDRALAB IV Joint User Meeting. HYDRALAB, Lisbon.

Arntsen, Ø.A., Obhrai, C., Gudmestad, O.T., 2013. "Data Storage Report: Wave Slamming Forces on Truss Structure in Shallow Water," WaveSlam (HyIV-FZK-05), Technical Report. Norwegian University of Science and Technology and University of Stavanger.

Choi, S.J., Lee, K.H., Gudmestad, O.T., 2015. The effect of dynamic amplification due to a structure's vibration on breaking wave impact. Ocean Eng. 96, 8–20.

Choi, S.J., 2014. Breaking Wave Impact Forces on an Offshore Structure (PhD thesis (UiS No. 231)). University of Stavanger, Norway, at the Department of Mechanical and Structural Engineering and Material Science.

Christensen, E.D., Bredmose, H., Hansen, E.A., 2005. Extreme Wave Forces and Run-up on Offshore Wind Turbine Foundations. Copenhagen Offshore Wind, Copenhagen.

Goda, Y., Haranaka, S., Kitahata, M., 1966. Study of Impulsive Breaking Wave Forces on Piles. In: Report of Port and Harbour Research Institute, vol. 5(6), pp. 1–30. Concept also in English language in Watanabe, A., Horikawa, K., (1974). Breaking wave forces on large diameter cell. Proc. 14th Intern. Conf. on Coastal Eng, 1741–1760.

Hirt, C.W., Nichols, B.D., 1981. Volume of fluid method for the dynamics of free boundaries. J. Comput. Phys. 39 (1), 201–225.

Hoque, A., 2002. Air Bubble Entrainment by Breaking Waves and Associated Energy Dissipation (PhD thesis). Toyohashi University Of Technology, Japan, at the Department of Architecture and Civil Engineering.

Huang, N.E., Zheng, S., Long, S.R., 1999. A new view of nonlinear water waves: the Hilbert Spectrum. Annu. Rev. Fluid Mech. 31, 417–457.

Hu, C., Kashiwagi, M., 2004. A CIP-based method for numerical simulations of violent free-surface flows. J. Mar. Sci. Technol. 9, 143–157.

Jose, J., Podrażka, O., Obhrai, C., Gudmestad, O.T., 2015. Experimental Analysis of Slamming Loads for the Truss Structures within the Framework of WaveSlam Project, Hydralab IV (http://www.hydralab.eu/project_publications.asp), Technical Report. University of Stavanger and University of Gdansk.

Jose, J., Choi, S.J., Lee, K.H., Gudmestad, O.T., 2016a. Breaking wave forces on an offshore wind turbine foundation (jacket type) in the shallow water. In: Proceedings of 26th International Ocean and Polar Engineering Conference, Rhodes, Greece, pp. 164–172.

Jose, J., Podrażka, O., Obhrai, C., Gudmestad, O.T., Cieślikiewicz, W., 2016b. Methods for analysing wave slamming loads on truss structures used in offshore wind applications based on experimental data. J. Offshore Polar Eng. 26 (2), 100–108.

Kamath, A., Chella, M.A., Bihs, H., Arntsen, Ø.A., 2016. Breaking wave interaction with a vertical cylinder and the effect of breaker location. Ocean Eng. 128, 105–115.

Lee, K.H., 2006. A Study on Time Domain Analysis of Nonlinear Dynamic Interaction Amount Waves, Currents and Bed Materials (PhD thesis). Nagoya University, Japan, at the Department of Civil Engineering.

Lee, K.H., Park, J.H., Baek, D.J., Cho, S., Kim, D.S., 2011. Discussion on optimal shape for wave power converter using oscillating water column. J. Korean Soc. Coast. Ocean Eng. 23 (5), 345–357.

Mo, W., Irschik, K., Oumeraci, H., Liu, P.L.F., 2007. A 3D numerical model for computing non-breaking wave forces on slender piles. J. Eng. Math. 58, 19–30.

Mo, W., Jensen, A., Liu, P.L.F., 2013. Plunging solitary wave and its interaction with a slender cylinder on a sloping beach. Ocean Eng. 74, 48–60.

Obhrai, C., Bullock, G., Wolters, G., Muller, G., Peregrine, H., Bredmose, H., Grune, J., 2004. Violent wave impacts on vertical and inclined walls: large scale model tests. In: Proceedings of the 29th International Conference on Coastal Engineering, vol. 1(4), pp. 4075–4086.

Sawaragi, T., Nochino, M., 1984. Impact forces of nearly breaking waves on a vertical circular cylinder. Coast. Eng. Jpn. 27, 249–263.

Tanimoto, K., Takahashi, S., Kaneko, T., Shiota, K., 1986. Impulsive breaking wave forces on an inclined pile exerted by random waves. In: Proceedings of 20th International Conference on Ocean Engineering, pp. 2288–2302.

Tang, L., Wai, O.W.H., 2016. Numerical study of air entrainment and bubble plume dynamics under breaking waves. In: Proceedings of 26th International Ocean and Polar Engineering Conference, Rhodes, Greece, pp. 669–672.

Wienke, J., Oumeraci, H., 2005. Breaking wave impact force on vertical and inclined slender pile-theoretical and large-scale model investigations. Coast. Eng. 52 (5), 435–462.